Mitt. Österr. Geol. Ges.	ISSN 0251-7493	93 (2000)	87-103	Wien, Juni 2003

Keywords
Thermal modeling
Metamorphic Core Complex
Exhumation of rocks
Penninic Windows
Normal fault

Effects of the geometry of normal faulting on the near surface heat flow during extension: the example of the Rechnitz Metamorphic Core Complex (Austria)

BERNHARD GRASEMANN[1] & ISTVÁN DUNKL[2, 3]

13 Figures, 2 Tables

Content

Abstract

The geometry of a normal fault has a first-order influence on the temperature history of the hanging wall and the footwall during extension. Two-dimensional thermal models show that the distribution of the magnitude of the near-surface heat flow after extension reflects the geometry of the normal fault. Three models where the footwall is exhumed by different velocity fields are investigated: (i) Models based on low-angle normal faults where the uplift of the footwall is compensated by erosion develop a higher geothermal gradient and consequently a higher near-surface heat flow in the footwall. (ii) Low-angle normal faults, which exhume the footwall by antiformal hinge line migration, result in higher near-surface heat flow values in the hanging wall. (iii) Normal faults with a more steeply dipping ramp that flattens to a horizontal detachment at depth reveal pronounced near-surface heat flow maxima centered near the fault trace after extension. In all models increasing rate of extension and faulting dip angle enhances the intensity of the near-surface heat flow.

Because the distribution of the magnitude of the near-surface heat flow is dependent on the geometry of the fault, geological methods that determine the temperature distribution of the hanging wall during normal faulting bear important tectonic information. Coal rank values and fission track ages were used to determine the cooling history of the hanging wall during exhumation of the Rechnitz metamorphic core complex. Currently available geological data suggest that the increased heat flow during normal faulting was localized near the margin of the exhuming metamorphic core. Therefore, we suggest that the normal fault responsible for the exhumation of the Rechnitz metamorphic core complex had a ramp-flat geometry.

Address of the authors

[1] Bernhard GRASEMANN, Institut für Geologische Wissenschaften, Universität Wien, A-1090 Vienna (Austria), E-Mail: Bernhard.Grasemann@univie.ac.at
[2] István DUNKL, Institut für Geologie und Paläontologie, Universität Tübingen, D-72076 Tübingen (Germany)
[3] István DUNKL, Laboratory for Geochemical Research, Hungarian Academy of Sciences, Budapest (Hungary)

Einfluss der Geometrie von Abschiebungen auf die Temperaturentwicklung in der oberen Kruste: Ein Beispiel vom Rechnitzer Metamorphen Kernkomplex (Österreich)

Zusammenfassung

Die Geometrie von Abschiebungen hat einen großen Einfluss auf die Temperaturentwicklung der Ober- (*hanging-*) und Unterplatte (*footwall*). Zweidimensionale thermische Computermodelle zeigen, dass die Wärmeflussverteilungen an der Oberfläche stark von der Geometrie der Abschiebung abhängt. Drei unterschiedliche Geometrien wurden untersucht: (i) Flache Abschiebungen mit Erosion der Unterplatte führen zu einem höheren geothermischen Gradienten und somit Oberflächenwärmefluss in der Unterplatte. (ii) Flache Abschiebungen, bei welchen die Unterplatte durch die Axialebene ihrer eigenen Biegung deformiert zeigen einen höheren Oberflächenwärmefluss in der Oberplatte. (iii) Listrische Abschiebungen mit einer steilen Rampe und flachem Horizont in der Tiefe resultieren in einem hohen Oberflächenwärmefluss in der Nähe des Ausbisses der Störung. In allen Modellen erhöhen schnellere Extensionsraten den Oberflächenwärmefluss.

Da die Verteilung des Oberflächenwärmefluss stark von der Geometrie der Abschiebung beeinflusst wird, können mit geologischen Methoden, welche die Temperaturverteilung in der Oberplatte während einer Abschiebung bestimmen, wichtige tektonische Schlüsse gezogen werden.

Inkohlungsgrad und Spaltspurdatierungen von der Oberplatte des Rechnitzer metamorphen Kernkomplexes werden hier als Anwendungsbeispiel diskutiert. Die vorhandenen geologischen Daten deuten auf einen erhöhten Wärmefluss in der Nähe des tektonischen Randes und somit könnte die Hauptstörung des Kernkomplexes eine steile Rampe und einen flachen Abschiebungshorizont in der Tiefe gehabt haben.

1. Introduction

Metamorphic core complexes represent regions where crustal-scale normal shear sense on a detachment brings mylonitized footwall rocks up from great depth and juxtaposes them beneath brittle deformed rocks of the hanging wall (DAVIS, 1983). Depending on the dip angle and the geometry of the normal fault the locus of uplift migrates through the footwall as the hanging wall is withdrawn. This process is commonly referred to as a "rolling hinge" mechanism (SPENCER, 1984; BUCK, 1988; WERNICKE & AXEN, 1988). Two kinematic end-members for this process have been described: the footwall denudation can either be accomplished by flexural failure (BUCK, 1988; KING & ELLIS, 1990) or by simple shear across steep planes (SPENCER, 1984; WERNICKE & AXEN, 1988). In order to investigate which process dominates the evolution of a metamorphic core complex, the knowledge of the detachment fault geometry is essential. AXEN & BARTLEY (1997) pointed out that the complexity of the "rolling hinge" mechanism and the associated transient physical processes make it difficult to translate geological observations and data into parameters constraining the geometry and kinematics of normal faulting. Ideally, multiple independent observations from both the hanging wall and the footwall are desirable.

Thermochronological studies of rocks from the footwall provide a powerful tool for revealing the cooling history. Based on the idea that different isotopic systems in minerals have different closure temperatures (DODSON, 1973), thermochronological methods like the *mineral pair method* (HARRISON et al., 1979) or the *altitude-dependence method* (e. g. WAGNER et al., 1977; FITZGERALD & GLEADOW, 1988) have been used in many tectonic studies in order to derive exhumation rate from cooling histories. However, many factors complicate the use of these methods (KETCHAM, 1996): temperatures at depth show a significant lateral variation and the isotherms are typically elevated below the surface fault tip. During exhumation, rocks from the footwall will pass through transient thermal conditions, and cooling of a given footwall sample accelerates in the upper crust assuming a constant slip rate. The age resolution of thermochronological methods as well as the uncertainties in the closure temperatures of individual isotope systems limits the use of these methods especially if slip rates are relatively high over geologically short time intervals. Two-dimensional numerical thermal models have been used in order to overcome these problems and to characterize the transient thermal frame of extending regions with different geometries and kinematics of exhumation (e. g. BUCK et al., 1988; RUPPEL et al., 1988; GRASEMANN & MANCKTELOW, 1993; KETCHAM, 1996, HOISCH et al. 1997).

Besides the investigations of pressure-temperature-time paths of rocks, the intensity and distribution of the near-surface heat flow provide another important tool with which detachment models can be tested (LACHENBRUCH et al., 1994; SASS et al., 1994, DUNKL et al. 1998). GRASEMANN & MANCKTELOW (1993) and TER VOORDE & BERTOTTI (1994) showed theoretically by means of thermal modeling that normal faulting with high exhumation rates in the footwall or high extension rates could produce warming of the adjacent hanging wall due to the rapid advection of heat. DUNKL et al. (1998) demonstrated with an example from the Rechnitz metamorphic core complex (RMCC, Eastern Alps, Austria), that normal faulting at various angles can easily provide enough heat flow for a thermal overprint of the hanging wall, which influences the apatite fission track (FT) ages. Increasing the rate of extension and fault dip angles enhances the intensity of the heat flow near the fault tip (BUCK et al., 1988).

In this study we will focus on the distribution of the near-surface heat flow in a profile normal to the tip line of a detachment fault. In the first part of this work, we show by means of a numerical thermal model that the near-surface heat flow distribution is strongly dependent on the geometry of the detachment fault and the erosion of the footwall. Therefore, actual measurements of surface heat flow above active normal faults may provide important information on the geometry of the detachments at depth. In a second part of this work we investigate the thermal overprint of the hanging wall of the RMCC. It should be emphasized that the models are not intended to provide a complete depiction of thermal evolution of the RMCC as the current available geological data still leave room for different interpretations and therefore, a number of processes that may be important are not considered.

2. Geometry and associated heat flow during normal faulting

In this discussion we investigate three different geometries of normal faulting and discuss the near-surface heat flow distribution after 5 Ma with 2 and 5 mm/a extension velocity respectively. These rates are chosen arbitrarily representing a slower and faster extension velocity. The temperature distribution within an 80 km wide and 30 km thick crust was calculated by solving the heat transfer equation (A1) in two dimensions using finite difference algorithm (Appendix and Tab.1). The upper surface has a constant temperature of 0 °C. The initial linear geothermal gradient is 20 °C/km. In the absence of advection of heat a steady state geothermal gradient is considered by using a boundary condition at the base of the crust with a constant heat flow of 61.6 mW/m^2, which is a result of conductivity given in Table 1. No heat production is considered in these calculations and therefore, only conduction and advection control the final temperature distribution (Note, that the models of the RMCC discussed below consider heat production!). These simplified conditions were chosen in order to emphasize the first-order effects of the geometry of the fault. In fact the distribution of radioactive elements influences the distribution of the heat flow **after** the metamorphic core has developed (LACHENBRUCH et al., 1994; SASS et al., 1994). Furthermore radioactive elements enriched in the upper crustal levels result in a non-linear geothermal gradient (e. g. TURCOTTE & SCHUBERT, 1982). The velocity components within the hanging wall (HW) are zero. The velocity field in the footwall (FW) depends on the initial geometry and slip rate (Fig. 1).

2.1 Low-angle normal fault with erosion of the footwall (Fig. 1a)

In this model the footwall moves with a uniform velocity w, which is equal to the extension rate, towards the surface. The velocity w has a horizontal component v_x (positive from left to right) and a vertical component v_z (positive downwards):

$$v_x = w\cos\alpha$$
$$v_z = -w\sin\alpha \qquad (1)$$

where α is the dip angle of the fault. There is a uniform elevation boundary condition at the surface, thus footwall material is removed when it reaches the upper boundary. The resulting erosion rate has the same value but its sense is opposite to the vertical velocity component v_z. As all velocity vectors within the footwall are equal in magnitude and direction the footwall is not deformed. Such simple geometries were applied to describe normal faulting in areas where significant footwall erosion has been reported (e. g. GRASEMANN & MANCKTELOW, 1993).

2.2 Low-angle normal fault with antiformal hinge migration (Fig. 1b)

In this model the velocity field in the footwall is divided by an axial plane (s_{ax1}) which bisects the angle between the

Table 1
Parameters, variables and physical constants used in the calculations for the models in Figures 2-5 and Figures 10-12 (Model I, II and III). For a detailed discussion of the model parameters see text.

symbol	description	models in Figs. 2-5	models I, II and III in Figs. 10-12
t	total time of model run	5 [Ma]	5, 10, 10 [Ma]
Δt	incremental time step	10000 [a]	10000 [a]
T	temperature	[K]	[K]
T_S	constant surface temperature	273 [K]	273 [K]
A	volumetric Heat Production	-	2.5^{-6} [W m^{-3}]
l	length of exponential decay of the heat production	-	30 000 [m]
κ	thermal diffusivity	10^{-6} [m^2/s]	10^{-6} [m^2/s]
C	specific heat	1100 [J/kgK]	1100 [J/kgK]
ρ	density	2800 [kg/m^3]	2800 [kg/m^3]
k	conductivity	3.08 [W/mK]	3.08 [W/mK]
q_s	Initial near-surface heat flow (0-1000m)	61.6 [mW/m^2]	92 [mW/m^2]
$q_m(t)$	mantle heat flux	61.6 [mW/m^2]	calculated from Eq. A7 [mW/m^2]
g	Initial geothermal gradient	20 [K/km]	calculated from Eq. A6 [K/km]
α	faulting dip angle	17° and 31°	10°, 20°, 30°
x, z	horizontal x vertical distance	80000 x 30000 [m]	100000 x 30000 [m]
Δx, Δz	grid spacing	500[m]	500[m]
v_x	velocity in x-direction	2 and 5 [mm/a]	11.3, 7, 7 [mm/a]
v_z	velocity in z-direction	variable [mm/a]	2, 2.55, 4 [mm/a]

fault and the footwall surface (180-α). The footwall below the fault moves with a uniform velocity *w* parallel to the fault plane with v_x and v_z components according to equation (1). Below the fault tip the footwall migrates through s_{ax1} causing the material to fold with a negative shear (RAMSAY & HUBER, 1987). Passing s_{ax1} the material continues to move horizontally and therefore, no material is eroded and no erosional topography is created in the footwall:

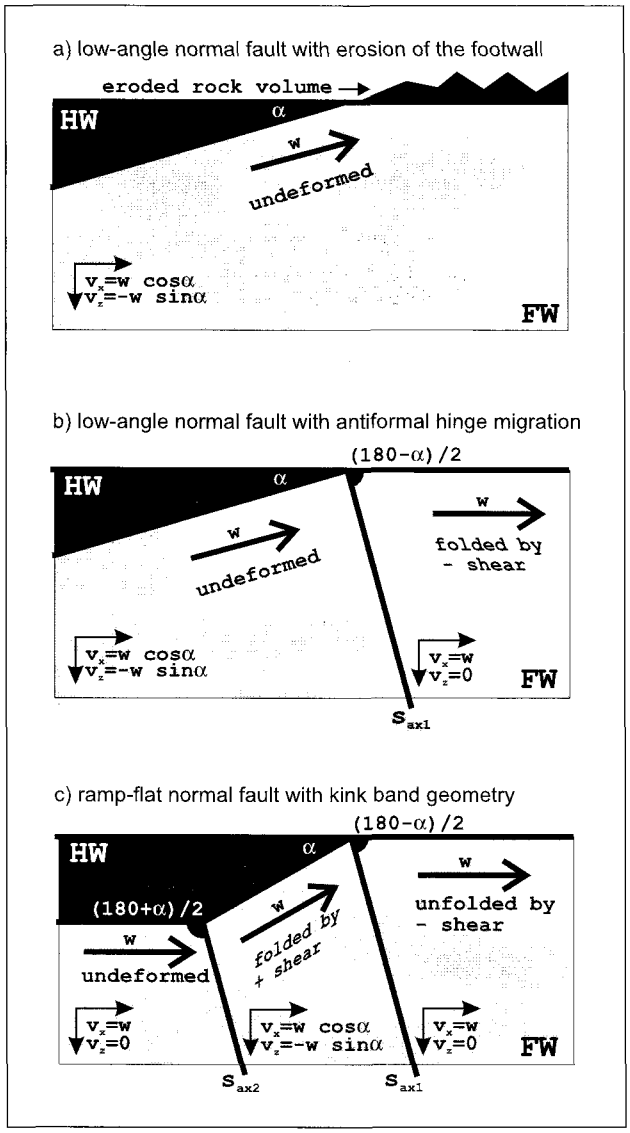

Fig. 1
Geometry of a (a) low-angle normal fault with erosion of the footwall (FW), (b) low-angle normal fault with antiformal hinge migration and (c) ramp-flat normal fault with kink-band geometry. In all models are the velocity components within the hanging wall (HW) zero. *a* is the dip angle of the fault. (a) The footwall moves with a uniform velocity *w* towards the surface where the footwall material is removed when it reaches the upper uniform elevation boundary. The resulting erosion rate is equal but opposite to the vertical advection rate v_z. (b) The undeformed material in the footwall below the fault migrates with the faulting velocity *w* through the axial plane s_{ax1} is folded by a negative shear. In (c) the undeformed material in the FW below the ramp migrates through the axial plane s_{ax2}, is folded by a positive shear. The faulting velocity *w* moves the material through the axial plane s_{ax1}, the material is unfolded by a negative shear.

$$v_x = w$$
$$v_z = 0 \qquad (2)$$

Although there are some differences in detail, this geometry is similar to other published models describing normal faulting (e. g. RUPPEL et al., 1988; BUCK at al., 1988; VAN WEES et al., 1992).

2.3 Ramp-flat normal fault with kink-band geometry (Fig. 1c)

The ramp-flat models approximate a geometry with a fault ramp that flattens to a horizontal orientation at a certain depth, a geometry commonly inferred in extensional zones (GIBBS, 1984; LISTER & DAVIS, 1989). Two footwall axial planes solve the geometric constraints: One axial plane (s_{ax1}) bisects the angle between the ramp and the surface on the footwall side (antiformal hinge), and the other axial plane (s_{ax2}) bisects the angle between the ramp and the horizontal detachment plane (synformal hinge). The footwall below the ramp migrates through s_{ax2} causing the material to fold with a positive shear. When the material passes through s_{ax1} rocks are unfolded by a negative shear. Note that in all three models all angles are kept constant. Because of the similarities between this geometry with models developed for the formation of kink folds (TWISS & MOORES, 1992) this geometry is called ramp-flat normal fault with kink-band geometry. The area between the synformal and antiformal axial plane is called the *kink band*. The terms *undeformed*, *folded* and *unfolded* are strictly used in a geometrical sense and are not mechanically correlated with an actual strain in the footwall. The velocity in the footwall below the flat and to the right of the fault tip has v_x and v_z components according to equation (2). The velocity components within the kink band below the ramp are calculated with equation (1).

This model combines the geometry suggested by the end-member models of flexural failure or rotation (BUCK, 1988; KING & ELLIS, 1990) and subvertical simple shear (SPENCER, 1984; WERNICKE & AXEN, 1988). Like in the flexural rotation model the axial planes bisect the angles at the antiformal and synformal hinges and thus the thickness of a given area in the footwall remains constant. However, there is no neutral surface in the footwall that separates areas with shortening and extensional strain respectively. Although the internal strain in the footwall is clearly different in these end-member models from the model chosen for the present study, the results of thermal calculations are similar within the range detectable by geological methods (AXEN & BARTLEY, 1997).

2.4 Results of the numerical thermal model

Figure 2 shows the temperature distributions after 5 Ma of normal faulting with a dip angle of 15° and with extension velocities of 2 and 5 mm/a respectively using the geometry of the low-angle normal fault model with erosion of the footwall (according to Fig. 1a). Although the whole modeled crustal section has an elevated geothermal gradient after the normal faulting, the heat flow is clearly higher in the footwall than in the hanging wall. This is a direct consequence of the vertical heat advection component and

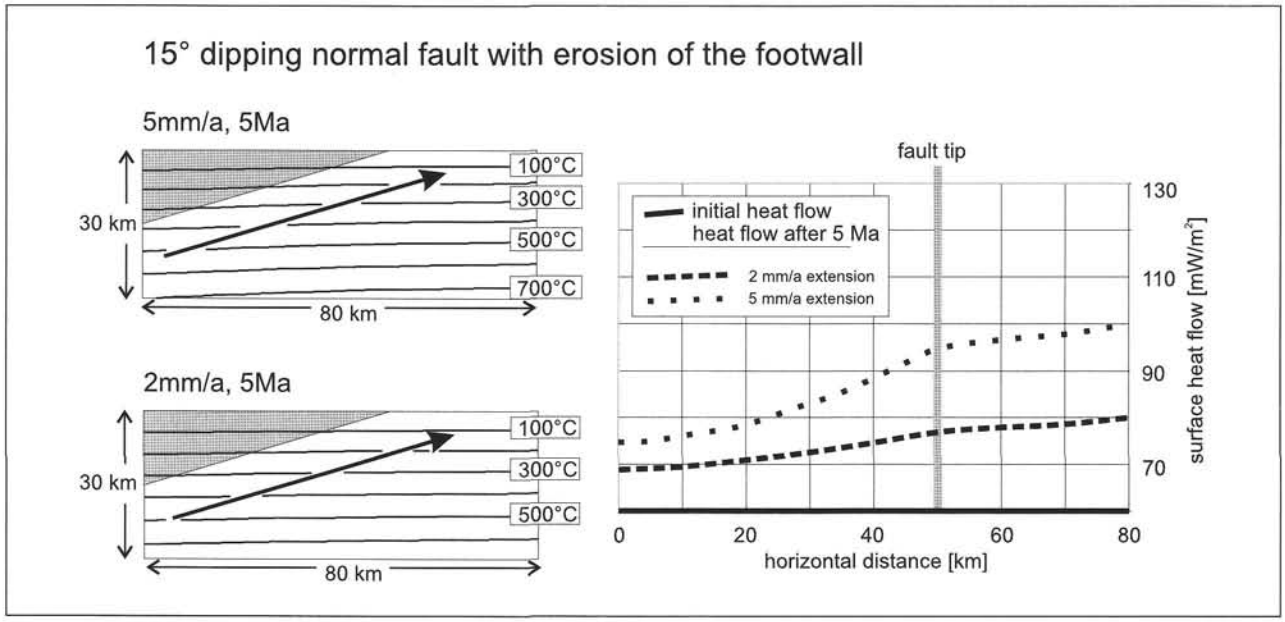

Fig. 2
Model results of a 15° dipping low-angle normal fault with erosion of the footwall considering no heat production. The temperature distribution within the crust is plotted after 5 Ma for extension velocities (v_x) of 5 and 2 mm/a. The diagram at the right shows the distribution of the heat flow after 5 Ma extension along a 80 km long section normal to the fault trace at the surface. Note that due to the erosion of footwall material the heat flow is higher on the footwall than on the hanging wall side. There is no peak heat flow near the fault tip.

(mathematical) erosion of material which only affect the footwall and which are zero in the hanging wall. Note, that there is also no sedimentation on the hanging wall. The temperatures in the hanging wall are only influenced by conduction of heat. The near-surface temperature distribution after faulting is shown in a plot horizontal distance versus heat flow (Fig. 2). The heat flow q is calculated using Fourier's law:

$$q = -k\frac{dT}{dz} \tag{3}$$

where k is the thermal conductivity (3.08 W/mK), T is the temperature and z is the depth (2000 m). Generally, depending on the faulting velocities, the heat flow in the footwall is about 10 to 20 mW/m² **higher** than in the hanging wall. However, there is no peak or step in the heat flow

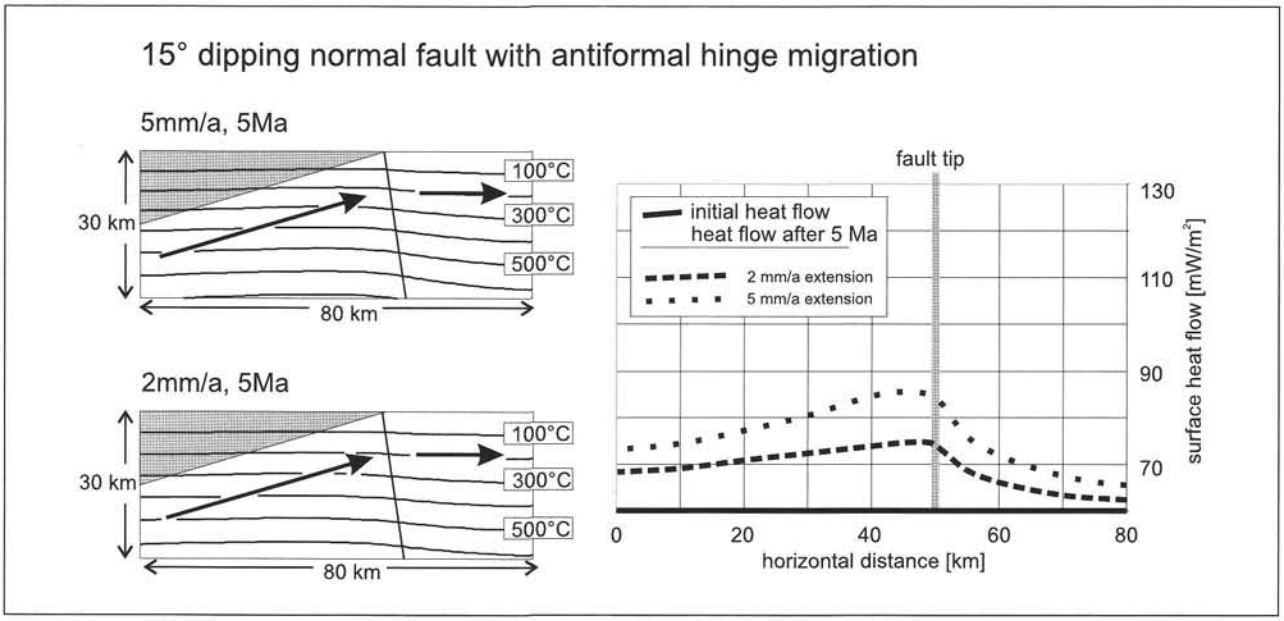

Fig. 3
Model results of a 15° dipping normal fault with antiformal hinge migration. The temperature distribution within the crust after 5 Ma extension shows a higher geothermal gradient on the hanging wall side of the fault tip. This can be also observed in the heat flow distribution curves, where the higher values are in the hanging wall. With higher extension rates (i. e. v_x >5 mm/a) a peak heat flow begins to develop within the hanging wall near the fault tip.

curves and without knowledge of the location of the fault tip it would be difficult to determine the transition from the footwall to the hanging wall.

Figure 3 shows the temperature distributions after 5 Ma of normal faulting with a dip angle of 15° and with extension velocities of 2 and 5 mm/a respectively using the geometry of the low-angle normal fault model with antiformal hinge migration (according to Fig. 1b). In fact this model is very similar to the model of Figure 2 except that there is no erosion of material. Passing through the antiformal hinge the velocity field has just a horizontal component and therefore, no heat is advected vertically. This dramatically affects the heat flow distribution across the fault. The near-surface heat flow in the hanging wall is quite similar to the previous model, reflecting the similar heat transfer process of conduction of heat from the "hotter" footwall. However, near the fault tip and in the footwall the heat flow drops, which is a direct consequence of the relaxation of the geothermal gradient after the material moves through the antiformal hinge. Depending on the slip rate, the heat flow in the footwall is about 10 to 20 mW/m² **lower** than in the hanging wall. Although there is no marked peak in the heat flow curve, the highest values are located within 10 km to the fault tip on the hanging wall side.

Figure 4 shows the temperature distributions after 5 Ma faulting on a ramp-flat detachment with a ramp dip angle of 30° and a horizontal flat. Extension velocities of 2 and 5 mm/a were modeled using the geometry of the ramp-flat normal fault model with kink-band geometry (see Fig. 1c). Below the flat detachment the material moves horizontally and consequently the initial geothermal gradient is undisturbed. Just near the ramp the geothermal gradient is slightly elevated due to conduction from the "hotter" kink band. When the footwall moves through the synformal hinge rocks start to exhume with velocities depending on the extension rate and the dip angle of the ramp (compare extension velocities of 5 and 2 mm/a and Fig. 4 and 5 where the dip angles are 30° and 55° respectively). Heat advected with the exhuming footwall causes isotherms to be arched and closer spaced near the surface below the fault tip. Higher exhumation *rates result in higher geothermal gradients within the kink* band. When the material passes through the antiformal hinge again no heat is advected because there is only a horizontal component in the velocity field and the geothermal gradient starts to relax. The heat flow distribution normal to the fault trace shows a marked centered peak at the fault tip. For extension velocities of 2 and 5 mm/a the heat flow within this zone is 20 and 40 mW/m² respectively higher than the initial values. These heat flow curves are very similar to the results of BUCK et al. (1988) showing a marked peak near the fault tip, a more shallow concave upwards part on the hanging wall side and a more steep concave upwards curve on the footwall side.

Figure 5 shows the same model as Figure 4 except the ramp dip is 55°. This steeper ramp results in a higher vertical component of the velocity field within the kink-band and consequently the geothermal gradients within this zone are for the same extension rates higher than in the previous model. A geometric consequence of these kink type models is that a steeper ramp results in shallow-dipping kink bands. The effects of a steep ramp on the temperature distribution can be observed in Figure 5: The kink-band and thus the zone of vertical advection is centered close to the fault tip but clearly on the footwall side. An interesting consequence of this type of geometry is that the location of the doming of the isotherms is dependent on the depth. The shallower part on the isotherms gradually move away from the hanging wall with depth. The near-surface heat flow curves show a marked peak near the fault tip but on the footwall side. The peak heat flow is about 40 mW/m² higher for 2 mm/a and more than 60 mW/m² higher for the 5 mm/a extension rate. However, the conductive thermal overprint of the hanging wall is less pronounced than in models assuming low-angle normal faults. The model in Figure 5 elevates the heat

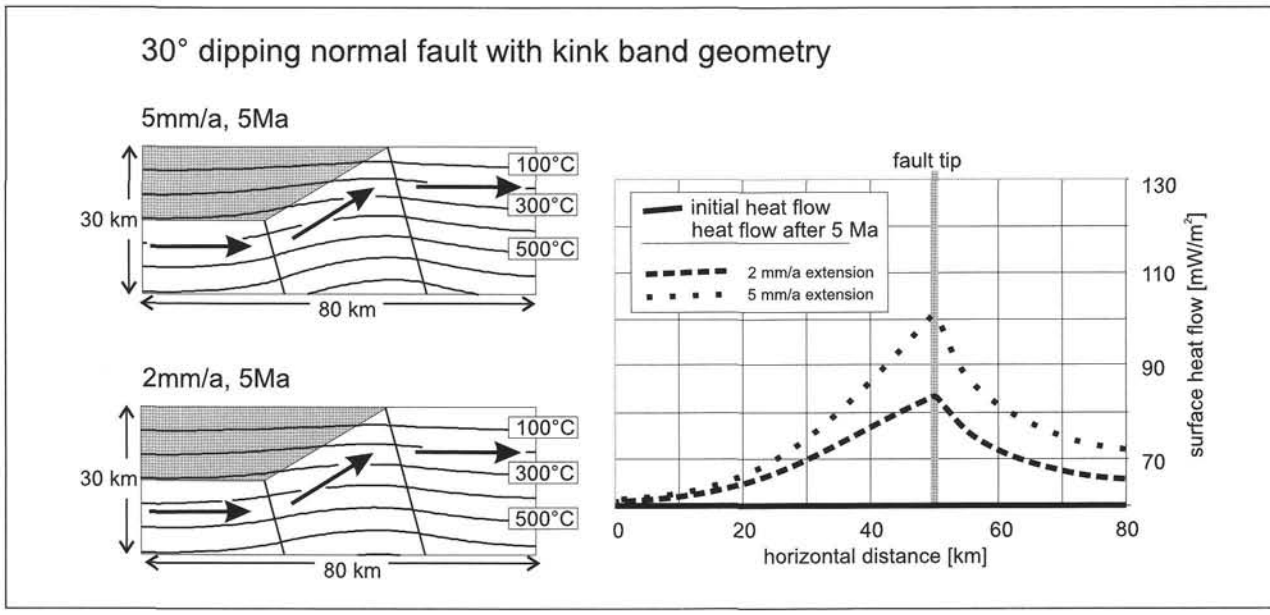

Fig. 4
Model results of a 30° dipping normal fault with kink-band geometry. The temperature distribution within the crust after 5 Ma extension shows a higher geothermal gradient within the kink band. The heat flow distribution curves show a marked heat flow peak, which is centered on the fault tip.

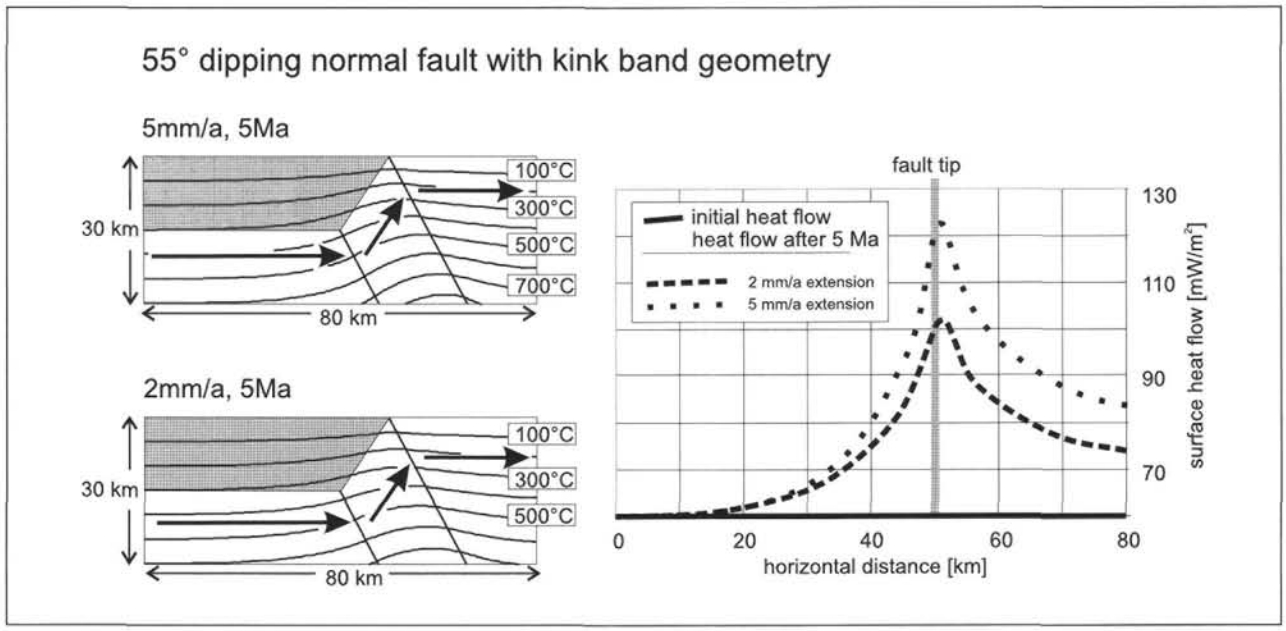

Fig. 5
Model results of a 55° dipping normal fault with kink-band geometry. The temperature distribution within the crust after 5 Ma extension shows that the location of the doming of the isotherms is dependent on the depth. The shallower part on the isotherms gradually move away from the hanging wall with depth. The near-surface heat flow curves show a marked peak near the fault tip but on the footwall side.

flow only about 30 km from the fault tip on the hanging wall side resulting in a steeper concave-upwards curve than heat flow curves on the footwall side.

2.5 Conclusions of the model results

(i) Erosion of the footwall results in a higher near-surface heat flow in the footwall (Fig. 2) whereas low angle normal faults with antiformal hinge migration have a higher heat flow in the hanging wall (Fig. 3). Both models have no marked heat flow peak near the fault tip.
(ii) Ramp-flat detachments show a heat flow maximum centered near the fault tip.
(iii) The conductive thermal overprint of the hanging wall is higher in ramp-flat models but restricted to a zone of a few tens of kilometers compared to low-angle normal faults.
(iv) Steep-dipping ramps have a narrow zone where the vertical advection of heat domes the isotherms whereas shallow-dipping ramps have a broad zone. If the same extension rates are applied, the vertical velocity component of broad kink bands is less than in narrow zones.

Bearing these considerations in mind we investigate the thermal overprint of the hanging wall above the Penninic RMCC in the Eastern Alps.

3. Application of the model on the Rechnitz Metamorphic Core Complex

3.1 Regional geology of the Rechnitz Metamorphic Core Complex

The Early-Middle Miocene evolution of the Eastern Alps was characterized by rapid exhumation of metamorphic core complexes (Tauern and Rechnitz Windows) and by magmatic activity (Styrian Basin). Both mechanisms caused elevation of transient geothermal gradients and near surface heat flow (Sachsenhofer, 2001). The RMCC represents the easternmost Penninic window of the Alpine chain, situated in the transitional zone of the Alps and the Pannonian basin (Fig. 6). It is the only Penninic window in the Alps, which is partly covered by Neogene syn-rift sediments (Fig. 7). The Penninic formations of the RMCC are mainly Mesozoic metasedimentary rocks with remnants of metamorphosed igneous rocks of ophiolitic origin (PAHR, 1980; KOLLER, 1985). The tectonic window structure of the RMCC (or strictly speaking a group of small windows) was formed during Early-Middle Miocene time (RATSCHBACHER et al. 1990). Greenschist facies metamorphism preceding the tectonic denudation ranged from 350 °C to 430 °C. Pressures are considered to have reached about 300 MPa (KOLLER, 1985). Thermochronological ages record only a short time span around 19 Ma and thus indicate relatively rapid cooling. K/Ar analysis of white micas give ages ranging from 22-19 Ma (W. FRANK pers. comm., 1992) whereas zircon FT ages from the exposed part of the RMCC give an average of 17.3 Ma (DUNKL & DEMÉNY, 1997). Younger apatite FT ages of 8-9 Ma express that during later phases cooling was distinctly slower.

Close to the RMCC the syn-rift Miocene Sinnersdorf beds show high coal maturation. The Sinnersdorf beds were deposited during exhumation, on top of the hanging wall not far above the main detachment of the RMCC. This very coarse, partly fanglomeratic sequence forms the basal part of the up to 3 km thick Early to Late Miocene clastic sequences (HERMANN & PAHR, 1988; PAHR, 1984; SCHÖNLAUB, 2000). The vitrinite reflectance values (Rr) range between 0.67 and 1.04% (SACHSENHOFER, 1991; EBNER & SACHSENHOFER, 1991). This post-depositional thermal overprint has been interpreted as a re-heating of the hanging wall due to

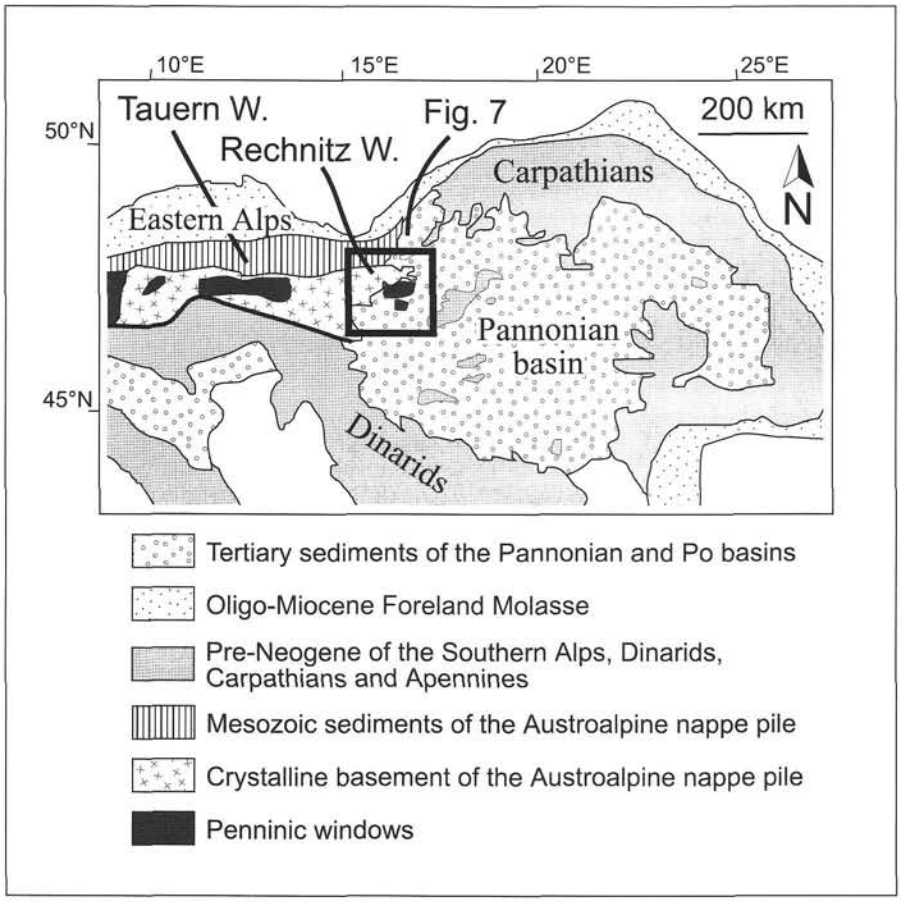

Fig. 6
Sketch map of the Alp-Carpathian-Pannonian region with location of the Rechnitz metamorphic core complex (RMCC, see Fig. 12).

advection of heat during rapid exhumation of the footwall (DUNKL et al., 1998, Sachsenhofer, 2001). The elevated geothermal gradient reset the apatite fission track ages in the sandstones and fanglomerates at the base of the sediment sequence. The average of 177 dated crystals is 13.6 ±0.9 Ma, which is clearly younger than the sedimentation age (around 19-17 Ma). A more detailed review of the data are given in DUNKL & DEMÉNY (1997) and DUNKL et al. (1998).

Due to the poor outcrop situation, the tectonic framework of the RMCC is less constrained than the well known structures of the Tauern Window where much of the information about the exhumation history is derived from structural, petrological and geochronological data of the footwall (e. g.: RATSCHBACHER et al., 1990; CLIFF et al., 1985; SELVERSTONE, 1985; von BLANCKENBURG et al., 1989). Therefore, we try to apply the simple models presented above with geologically more realistic initial and boundary conditions investigating the varying grade of thermal maturation and resetting of FT ages in the sediment cover of the hanging wall of the RMCC. However, we are aware that the simplifications of the presented models as well as the current available geological data from the RMCC are far from well constrained and should be understood as an illustration of the effects of the geometry of normal faulting on the near surface heat flow during extension.

3.2 Initial conditions and model parameters

The angle of the detachment of the RMCC is unknown. Therefore, the dip of the fault plane considered in the following models is either a low-angle fault (i. e. 10°, Model I) or a ramp with a dip of 20° (Model II) and 30° (Model III) and a horizontal detachment at a depth of 10 km (Tab. 1). The proposed geometry, the ramp angles and the depth of the horizontal detachment are very similar to models suggested for the Brenner Line at the western margin of the Tauern Window (SELVERSTONE et al., 1995), where postmylonitic structures suggest that isostatically driven footwall exhumation was accomplished by predominantly subvertical simple shear.

Deformation of the lower crust occurs predominantly by ductile flow and prevailed in the Penninic unit (RATSCHBACHER et al., 1990). Based on the study of delay time of teleseismic P-waves and the combination with results from magnetotelluric soundings the current thickness of the lithosphere below the RMCC is considered to be between 100 and 120 km and increase to 150 km to the west (PRAUS et al., 1990; HORVÁTH, 1993). This thinning was probably caused by the Neogene stretching event that affected the entire Eastern Alps (RATSCHBACHER et al., 1991) modifying the thermal structure of the crust (Sachsenhofer, 2001). The models discussed here use constant depth – variable heat flow (STÜWE & SANDIFORD 1995) at the base of a 30 km thick crust (HORVÁTH 1993 and references cited therein) in order to model the effects of the Neogene thinning of the lithosphere. The heat flow is determined by the function:

$$-k\frac{dT}{dz} = q_m(t) \qquad (4)$$

where k is the conductivity, T the temperature and $q_m(t)$ a time-dependent function. This lower boundary condition function allows the approximation of the effect of advection

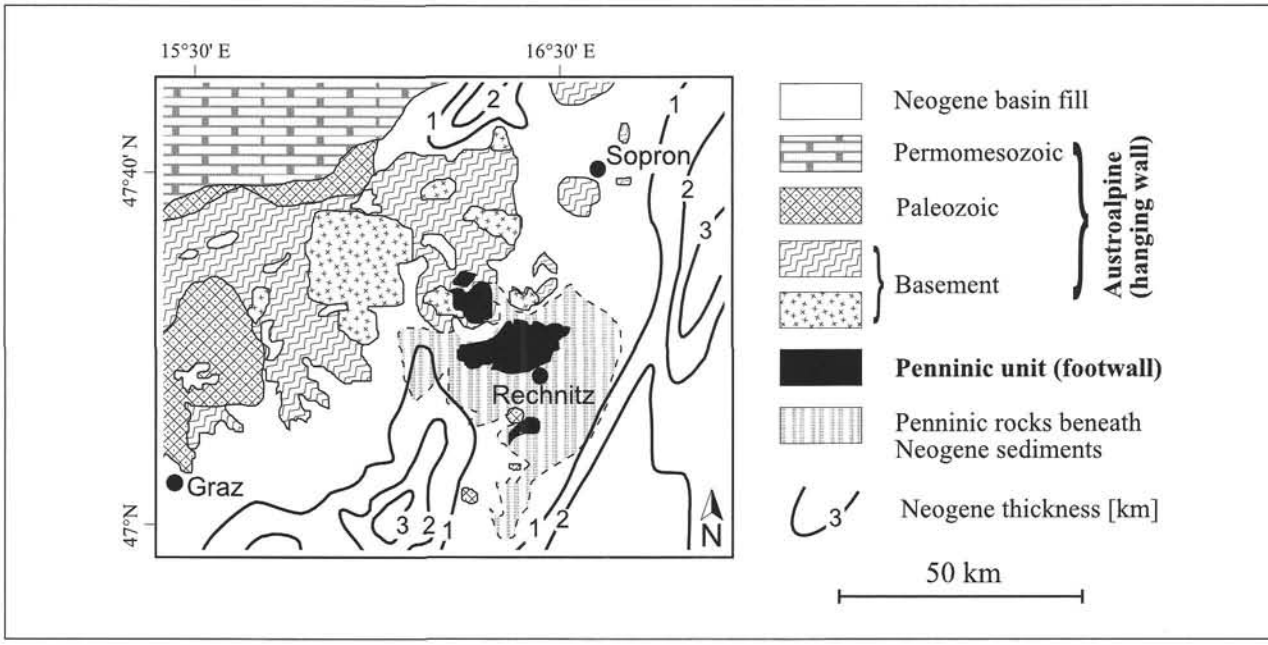

Fig. 7
Cartoon map of the surrounding of the RMCC. Dashed line shows the contour of the window below the syn- and post-rift Neogene sediment cover (after FLÜGEL & NEUBAUER, 1984; NEUBAUER & FRISCH, 1993 and TARI & HORVÁTH, 1995).

by faulting in the crust and by pure shear thinning in the mantle. The changing heat flow at the basal boundary condition is applied as a function of time $q_m(t)$ calculated with an analytical solution (MANCKTELOW & GRASEMANN, 1997) of the one-dimensional heat diffusion equation (CARSLAW & JAEGER, 1959) considering that the exhumation rate and the heat production may vary in space and time (Appendix). However, this study focuses on the near-surface heat flow and several model runs with different lower boundary conditions revealed very little impact on the results presented in this work.

TARI (1994) suggested that the horizontal component of extensional faulting of the RMCC is approximately 80 km. His calculations are based on the structures, the estimated size of the Penninic outcrops and from the distance between the disconnected Alpine nappes in the hanging wall (TARI & HORVÁTH, 1995). However, the hanging wall has suffered a complex Eo-Alpine history that was terminated by pronounced Late Cretaceous extension (MÜLLER et al., 1992; NEUBAUER et al., 1995). Furthermore not all of the displacement was accommodated at the western side of the RMCC and therefore, the modeled total horizontal displacement is shorter than TARI'S(1994) estimation: the low-angle fault model (Model I) has a finite stretch of 1.565; the ramp-flat models (Model II and III) have a finite stretch of 1.7. These stretching values correspond to a horizontal

Fig. 8
Plot of the dependence of vitrinite reflectance and track annealing in apatite on the temperature and effective heating time (after GLEADOW et al., 1983). Gray belt represents the field of partial stability of tracks in apatite. The temperature-duration field of the thermal overprint is controlled by the followings: (1) difference of sedimentation age and the apparent FT age proves that the duration was between 3 and 5 Ma; (2) the coal rank values (SACHSENHOFER, 1991) determine the maximum temperature; (3) the top of the partial stability zone marks the minimum temperature – as the single crystal apatite FT ages of the overprinted sediments show total resetting (DUNKL et al., 1998).

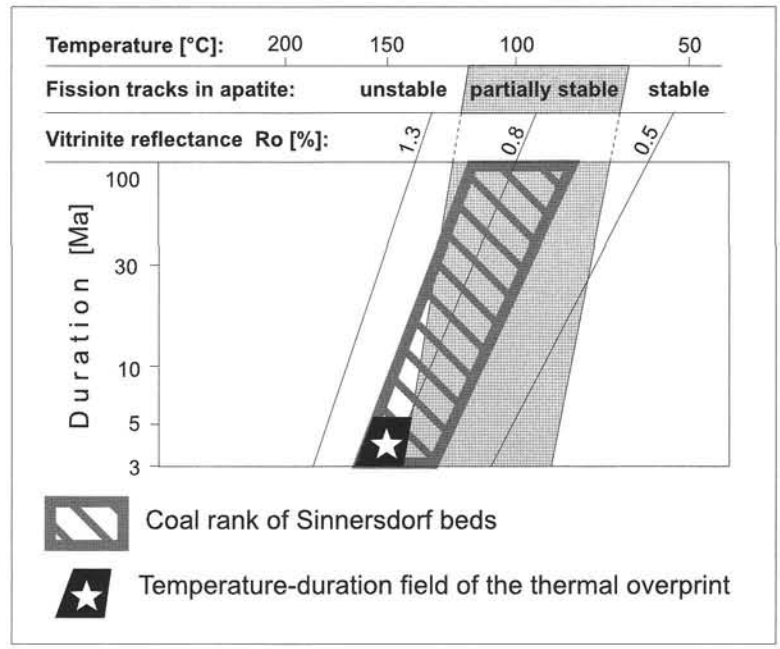

component of extensional faulting of 56.5 and 70 km respectively.

Although the Sinnersdorfer beds form locally an up to 3 km thick clastic sequences, syn-extensional sedimentation on the hanging wall of the RMCC is not considered in the models and assumed to have minor effects on the thermal structure on the scale of the whole crust. Therefore, the model setup presumes that sedimentation did not to result in a significant thickening of the hanging wall but accommodated extension and local graben formation.

The cooling rate of the Penninic rocks (i.e. the footwall) was rapid during Early-Middle Miocene times (DUNKL & DEMÉNY, 1997). This coincides with the time of rapid cooling of the Penninic rocks in the Tauern Window (CLIFF et al., 1985; von BLANCKENBURG et al., 1989) and in the Lepontine dome- Cental Alps (see reviews in PURDY & JÄGER, 1976; WAGNER et al., 1977; GRASEMANN & MANCKTELOW, 1993). In the models presented below, the period of rapid extension is between 22 and 17 Ma (Model I) and 27 and 17 Ma (Model II and III). The temperature history outside this interval is discussed but due to the lack of precise data it is not modeled in detail. Note that the geochronological data are not very tightly constrained. Therefore, the presented models are just examples that outline the first-order effects of the different models.

Apatite FT ages from the syn-rift sediments deposited on the hanging wall of the RMCC are younger than the age of sedimentation, due to a post-depositional thermal overprint that annealed the pre-existing tracks. The average age is 13.6 Ma. The zircon FT ages from the same localities are not reset by the thermal overprint (DUNKL et al., 1998) and give a mean in early Eocene time. Therefore, the modeled temperature history of the hanging wall is not allowed to rise above the closure temperature of zircon (240 ±50 °C; HURFORD, 1986) but must be above the apatite partial-annealing zone (~120 °C; WAGNER et al., 1977). Fig. 8 shows the possible temperature-duration field of the thermal overprint of the dated samples, constrained by the observed organic maturation (SACHSENHOFER, 1991) and track stability data (GLEADOW et al., 1983). Thermal modeling (KETCHAM et al., 2000) of fission track data of the reset sediment samples yielded a relatively simple cooling path (Fig 9). The rapid decrease in temperature between 14 and 12 Ma ago can be attributed to final cooling after the cessation of normal faulting, the consequent relaxation of the elevated geothermal gradient and an erosional event that affects the hanging wall by removing the upper part of the sedimentary pile.

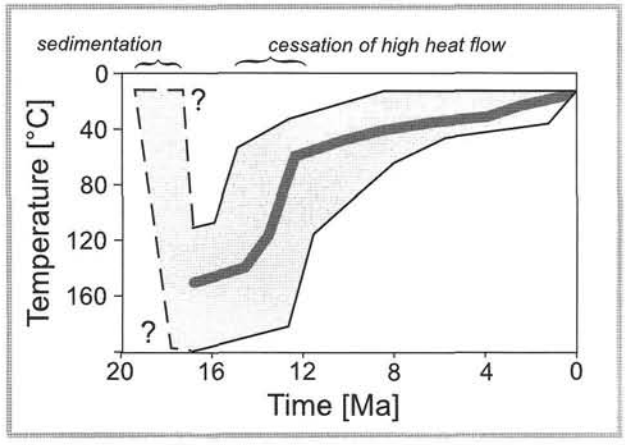

Fig. 9
Cooling path of the thermally overprinted Early Miocene sediments generated by AFTSOLVE program (KETCHAM et al.2000), based on fission track data (DUNKL et al., 1998). Chlorine content of 0.1 wt.% was considered and the annealing model of DONELICK et al. (1999) was used. Light gray field represents the envelope of the acceptable paths, gray line in the middle of this field is the tT path of the best modeling run.

3.3 Model results

The heat transfer equation (A1) is solved numerically over a two-dimensional finite difference grid with a horizontal distance x of 100 km and a positive downwards distance z of 30 km (Appendix, Tab. 1). The equally spaced grid resolution is 500 m. The initial temperature distribution is calculated with equation (A7) using physical parameters listed in Table 1. This grid describes a cross-section parallel to the dip-slip movement of the normal fault. Depending on the model configuration (Fig. 1) the velocity components v_x and v_z describe the velocity field within the footwall (equation 1 and 2).

3.3.1 Model I

Model I is a low-angle normal fault with antiformal hinge migration (according to Fig. 1b) with a fault dip angle of 10° (Fig. 10a). The sample in the footwall (SF) is located at a depth of 15 km below the surface and has an initial temperature of 380 °C. The horizontal and vertical velocity components are 11.3 mm/a and 2 mm/a respectively. During the simulation of 5 Ma the sample is moved to position SF' at a depth of about 5 km and cools down to 200 °C. The sample SH located at a fixed grid point in the hanging wall at a depth of 2.5 km has an initial temperature of about 75 °C and 120 °C after 5 Ma extension. Within the footwall advected hot material replaces initially colder crust below the fault plane. The hanging wall above the fault is slowly heated indicating an overall increase of the geothermal gradient caused mainly by conduction from the advected heat from the footwall. The highest geothermal gradient after the period of rapid exhumation is not below the fault trace or within the metamorphic core but about 5 km from the fault tip on the hanging wall side (indicated by a candle in Fig. 10a).

Figure 10b shows the near-surface heat flow (calculated with equation 3) over the horizontal distance of 100 km. The initial heat flow is about 92 mW/m² resulting from the assumed conductivity in Table 1 and is constant over the solution domain. The heat flow after 5 Ma faulting rises in the hanging wall from around 105 mW/m² at 80 km from the fault tip to 135 mW/m² at 5 km. Because the exhumation rate in the window itself – where the footwall moves horizontally – is zero, the near-surface heat flow rapidly relaxes again to lower values (around 105 mW/m²). Although the maximum heat flow is roughly centered on the hanging wall side near the fault trace the heat flow distribution shows a pronounced asymmetry.

Figure 10c shows a temperature-time plot with the approximate distribution of white mica K/Ar, zircon and apatite FT data from the footwall (gray boxes; DUNKL & DEMÉNY, 1997) and apatite FT data from the overprinted sedimentary cover of the hanging wall (stripped belt; DUNKL et al., 1998). The solid curves show the modeled cooling curves during the period of rapid faulting of the hanging wall and footwall

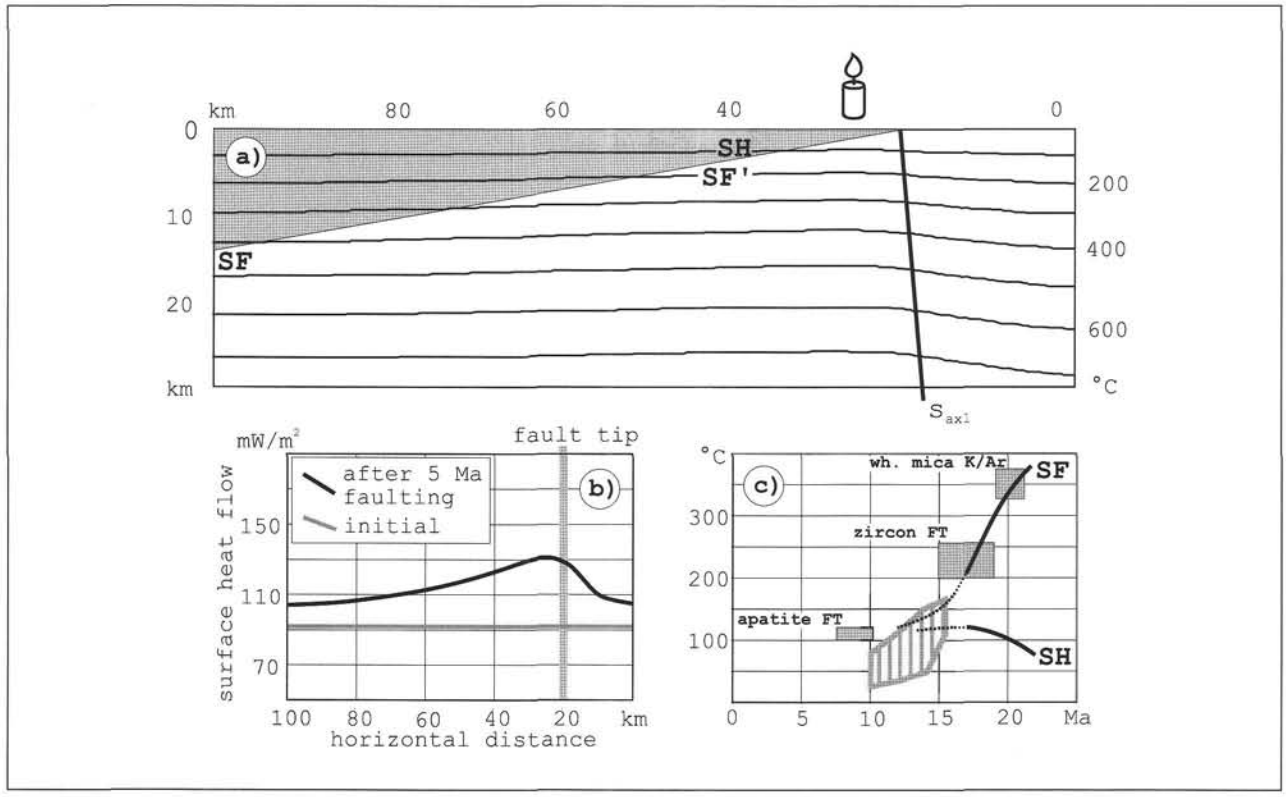

Fig. 10
Model results of the low-angle normal fault model with a fault dip angle of 10°. The horizontal and vertical velocity components are 11.3 mm/a and 2 mm/a respectively. (a) Isotherms after 5 Ma normal faulting. The candle indicates the position of the highest geothermal gradient. SF and SF' are the positions of the rock sample in the footwall before and after the period of rapid faulting. SH is the position of the stationary sample of the hanging wall. (b) Near-surface heat flow over the horizontal distance of 100 km normal to the fault trace. The initial heat flow is about 92 mW/m² and constant over the modeled distance. The near-surface heat flow after 5 Ma faulting has a peak 5 km to the hanging wall side of the fault trace with 135 mW/m². The heat flow values are asymmetric around the peak. The thermal overprint of the hanging wall with values above 110 mW/m² affects a zone up to 40 km distance to the fault trace. (c) Modeled cooling curve (solid lines) for the hanging wall and the footwall samples (SH and SF, respectively). Further explanations see text.

samples (SH and SF) respectively. Whereas the footwall shows a rapid, slightly convex upward cooling from about 380 to 200 °C, the hanging wall heats from about 75 to 120 °C. The dashed curves show a probable continuation of the cooling history. However, this is not numerically modeled because of the current lack of precise geological data. The suggested cooling path after 17 Ma would represent a continuation of the fault movement but at a slower rate. This Late Miocene, less intense extensional phase is well documented in the seismic profiles of Styrian basin and the western Pannonian basin (EBNER & SACHSENHOFER, 1991; TARI, 1994). A slower rate of normal faulting after a period of rapid movement or a decrease in the faulting velocity has been observed also at the Simplon normal fault, where the cooling curves of hanging wall and footwall are much more precisely defined (GRASEMANN & MANCKTELOW, 1993). Due to the relaxation of the geothermal gradient after the onset of slower advection the sample from the footwall would initially continue to cool at a faster rate but the cooling would decrease creating a concave-upward shape of the cooling curve. The rocks in the hanging wall would maintain their high temperatures due to the continued conduction of heat from the still hotter footwall. Whereas a certain amount of cooling in the hanging wall can be caused by the relaxation of the overall geothermal gradient, the sample can only approach the surface by erosion of the hanging wall.

A different, and for the RMCC, probably more realistic tectonic history would be controlled by excisement or cutting up of the detachment fault through the hanging wall, which is a frequent feature in core complexes (e. g. WERNIKE & AXEN, 1988; LISTER & DAVIS, 1989). However, the topology of the cooling curves would be quite similar depending on the timing of excisement: The hanging wall would first show heating followed by cooling after excisement, while the footwall points follow a continuous cooling path (KETCHAM, 1996).

3.3.2 Model II

Model II is a ramp-flat normal fault with kink band geometry (according to Fig. 1c) with a ramp dip angle of 20° and a horizontal detachment at a depth of 10 km (Fig. 11a). The sample in the footwall (SF) is located at a depth of 11 km below the detachment at the left border of the modeled geometry and has an initial temperature of 289 °C. The horizontal and vertical velocity components within the kink band geometry are 7 mm/a and 2.55 mm/a respectively.

In order to achieve a horizontal component of extensional faulting of 70 km the model run takes 10 Ma. During this time span the sample is moved to position SF' at a depth of about 5 km and cools down to 200 °C. The sample SH located at a fixed grid point in the hanging wall at a depth of

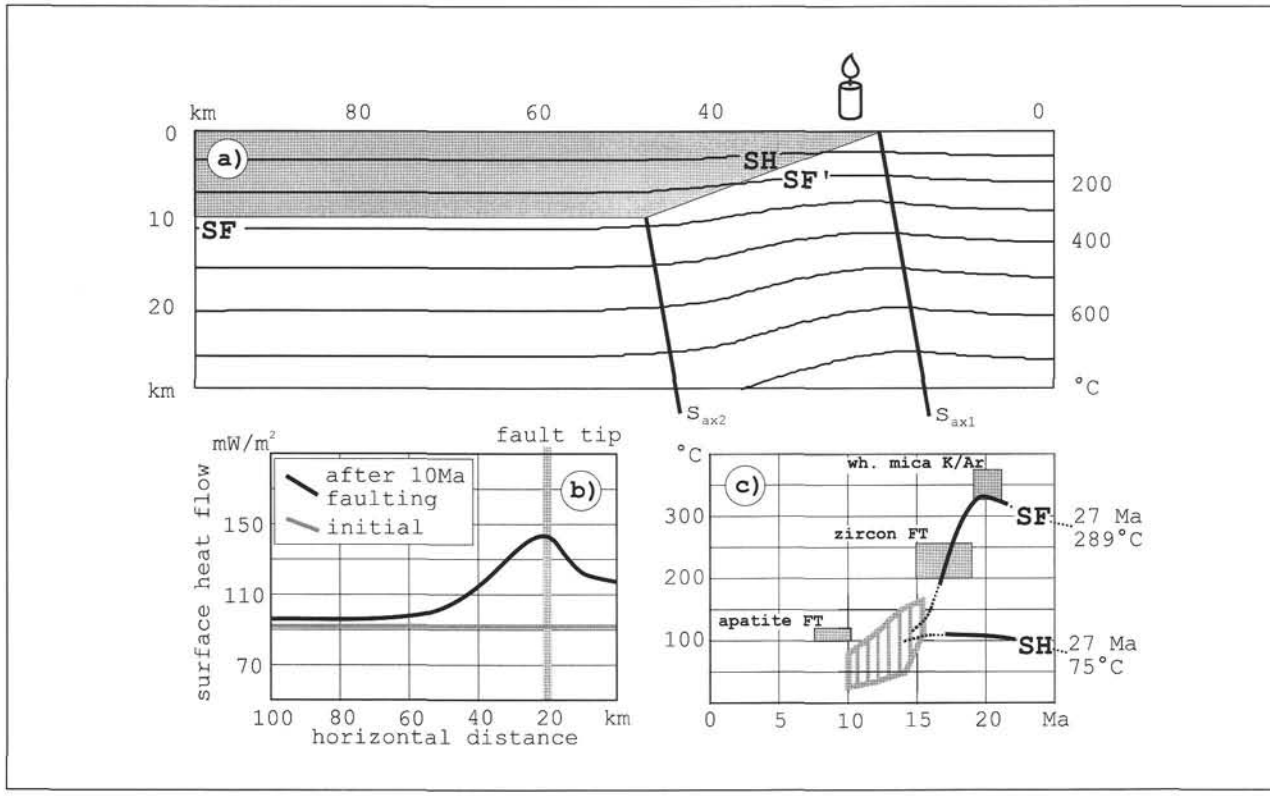

Fig. 11
Model results of a ramp-flat normal fault model with a ramp dip angle of 20°. The horizontal detachment is located at 10 km depth. The horizontal and vertical velocity components are 7 mm/a and 2.55 mm/a respectively. (a) Isotherms after 10 Ma normal faulting. SF and SF' are the positions of the rock sample in the footwall before and after the period of rapid faulting. SH is the position of the stationary sample of the hanging wall. (b) Near-surface heat flow over the horizontal distance of 100 km. The initial heat flow is about 92 mW/m² and constant over the modeled distance. In the hanging wall, values higher than 110 mW/m² are restricted to a zone of 20 km on the hanging wall side of the fault tip. (c) Modeled cooling curve (solid lines) for the hanging wall and the footwall. Further explanations see text.

2.5 km has an initial temperature of about 75 °C and heats up during the model run to 130 °C.

A direct consequence of the ramp-flat geometry is that the material and the heat is advected with a vertical component only beneath the ramp between s_{ax1} and s_{ax2}. Nevertheless, the geothermal gradient after extension below the fault tip is slightly higher than the gradient measured at the same position in Model I where the whole footwall below the normal fault experiences a vertical advection component. The slightly higher vertical velocity component and the longer time period of extension can easily explain the higher maximum temperatures of Model II. However, as can be seen in the near-surface heat flow plot normal to the fault trace, values higher than 110 mW/m² are restricted to 20 km on the hanging wall side (Fig. 11b). In the low-angle normal fault model (Model I) this thermal overprint with values above 110 mW/m² affects the hanging wall up to 40 km from the fault trace.

Figure 11c shows a temperature-time plot similar to that in Figure 10c. The solid curves show the temperature history of the same time interval (i. e. 22-17 Ma) considered in Model I in order to compare the modeled cooling curves. Note, however, that the model run of Model II starts 5 Ma earlier. Although, the available geochronological data would not be able to distinguish between Model I and II, there is a marked and very important difference in the cooling histories between the two models. The footwall sample SF of Model I start its exhumation history at a temperature of 380 °C (presumably its maximum temperature) and is subsequently cooled. Therefore, SF has its peak temperatures **before** the period of rapid normal faulting. The footwall sample SF in Model II starts at 289 °C and is heated up to 330 °C before it starts cooling. During the first 8 Ma the sample moves from a depth of 11 km (its starting depth) parallel to the detachment. Because this path is parallel to the isotherms the sample experiences no temperature change. When the sample approaches the synformal hinge it is heated by horizontal conduction from underneath the ramp. As the sample moves through the axial plane s_{ax2} the velocity field changes and the sample starts to cool because it is exhumed through the elevated geothermal gradient beneath the ramp. Thus the exhuming sample in the ramp-flat model reaches its peak temperatures **during** normal faulting.

3.3.3 Model III

Model III is identical to the model configuration of Model II described above except that the ramp dip is 30°. The horizontal and vertical velocity components are 7 mm/a and 4 mm/a respectively. This slightly higher exhumation rate results in generally higher geothermal gradients below the ramp (compare Fig. 11a and 12a). The temperatures measured after extension below the fault tip are around 50 °C warmer from mid crustal levels down to the Moho than in Model II with the lower exhumation rates. However, the kink-

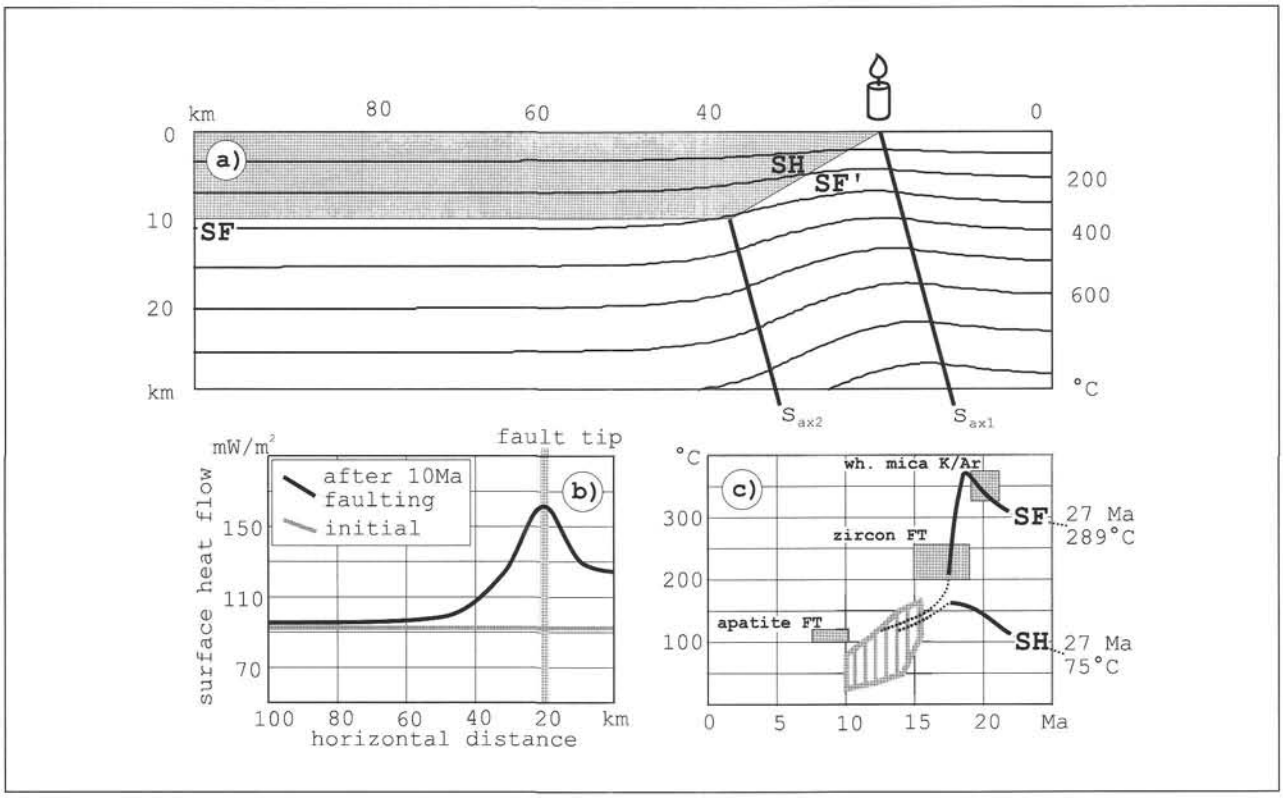

Fig. 12
Model results of a ramp-flat normal fault model with a ramp dip angle of 30°. The horizontal detachment is located at 10 km depth. The horizontal and vertical velocity components are 7 mm/a and 4 mm/a respectively. (a) Isotherms after 10 Ma normal faulting. (b). The near-surface heat flow curves show a pronounced peak of 160 mW/m² which is centered on the fault trace. In the hanging wall, values higher than 110 mW/m² are restricted to a zone of 16 km on the hanging wall side of the fault tip. (c) Modeled cooling curve (solid lines) for the hanging wall and the footwall. Further explanations see text.

band width and thus the zone where the heat advection has a vertical component is 30 km and 20 km in Model II and III respectively. This narrow zone of footwall uplift results in a pronounced peak in the heat flow versus distance to fault tip plot (Fig. 12b). A clear peak up to 160 mW/m² symmetrically arranged within a few km around the fault trace is observed. The difference in heat flow at some distance to the fault trace between the hanging wall and the footwall is dramatic. Whereas the heat flow in the hanging wall is only about 95 mW/m² the values in the footwall are 30 mW/m² higher. However, the width of the zone where the hanging wall is thermally overprinted with a near-surface heat flow above 110 mW/m² is less than 16 km.

3.4 Evaluation of model and geological data

The Austroalpine hanging wall underwent a Late Cretaceous metamorphism, which reached amphibolite facies grade in some places. The zircon FT ages generally range between 77 and 55 Ma and thus record the cooling of the Late Cretaceous metamorphic event (BALOGH & DUNKL, submitted). The apatite FT ages, however, show pronounced regional differences around the RMCC (Fig. 13a). North of the window there is a roughly E-W trending belt of ages between 60 and 30 Ma. In this zone the integrated depth of post-Cretaceous erosion is relatively shallow. South of this belt, between the Pannonian basin and the Paleozoic of Graz – including the immediate frame of the window – the range of apatite ages is much younger (16-10 Ma) related to the Miocene extension and elevation of the geothermal gradient (Sachsenhofer, 2001). However, the 50 km long and 30 km wide belt of young apatite ages did not suffer significant exhumation. The widespread Miocene ages were formed by the combination of erosion with increased heat flow and the vertical thinning probably due to excisements of the detachment fault through the hanging wall during extension. An extremely old apatite apparent age (GP-21 sample, 61±8 Ma; see Fig. 13a and Tab. 2) proves that inside the area of young apatite ages there are tilted blocks with preserved high level. The proximity of Middle Miocene apatite FT ages in the hanging wall (~7 km) and the margin of Penninic window (~4 km) to the locality of GP-21 sample highlight the importance of this extremely old FT age and reflect the complexity of the region.

Miocene sediments are only preserved in isolated occurrences, but numerous intramontane basin remnants (see Fig. 7) give evidence that erosion was limited. The region of the RMCC was not a topographic high during extension, but mainly covered by sediments. In the neighborhood of the core complex the apatite FT ages in the syn-rift sediments are reset. Other samples (e. g. GP-19, located ~8 km west of the margin of the window) show no significant resetting. The apatite FT single-grain ages are much older than the age of deposition. At these localities the Miocene burial temperature were not able to anneal the inherited pre-Miocene ages –although, we may not exclude a slight, insignificant rejuvenation (Tab. 2, Fig 13b).

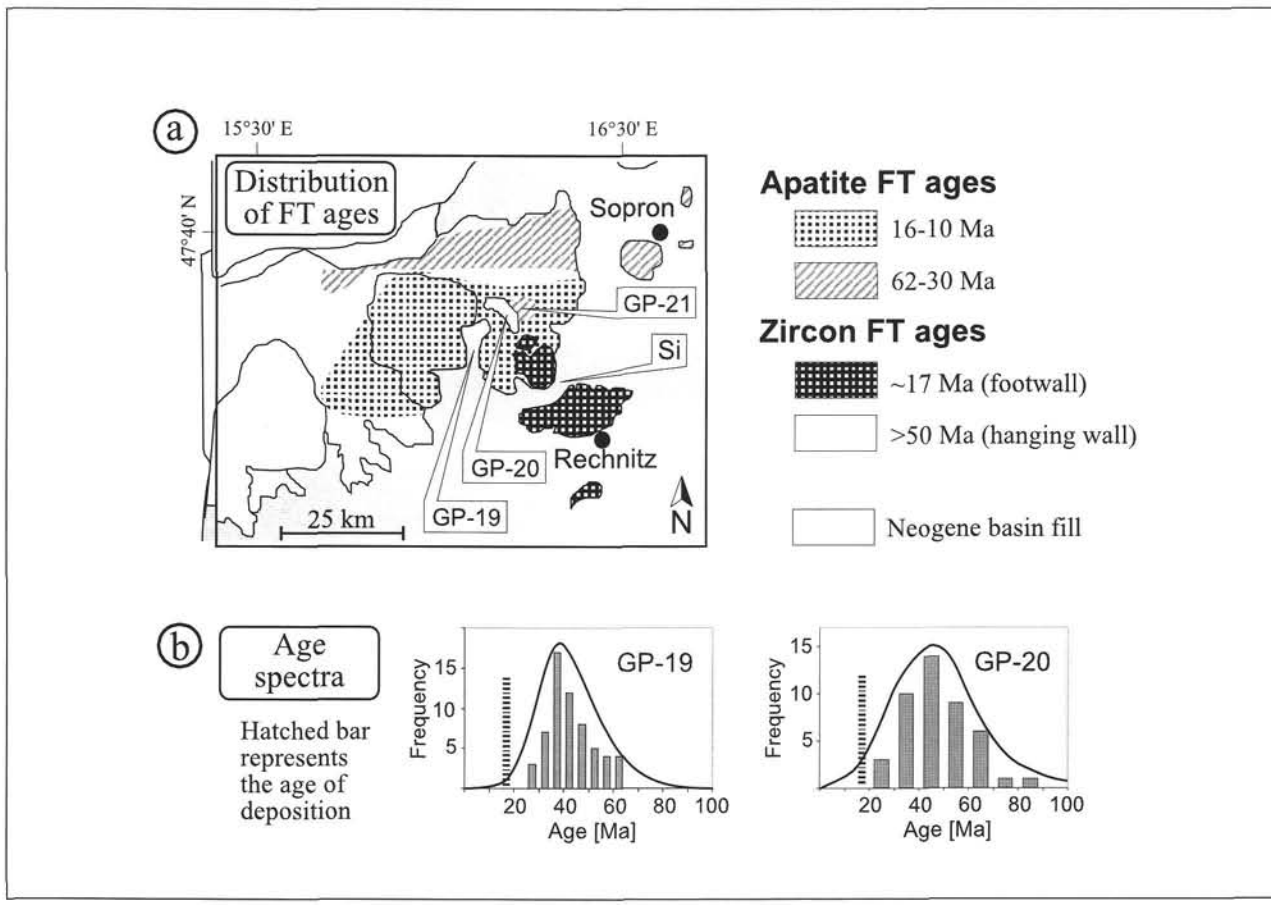

Fig. 13
(a) Contours of the pre-Miocene and Miocene apatite fission track ages. GP- sample numbers (see Tab. 2); Si: – Sinnersdorf beds. (b) Age spectrum of an Early Miocene conglomerate sample (GP-19), where the thermal overprint was negligible. The single grain apatite FT ages are expressing the Paleogene cooling age of the source area of the sediment.

Coal petrographical studies have proved that post-depositional overprint is localized only to the boundary of the core complex (EBNER & SACHSENHOFER, 1991; BELOCKY et al., 1991). Samples of similar depositional ages close to the base of the Neogene sedimentary pile further west of the window do not show significant overprint.

The interpretation of the currently available geological data suggests that the increased heat flow during normal faulting was localized near the margin of the exhuming metamorphic core. The presented models show that heat flow peaks centered near the fault trace are typical for normal faults with a roughly horizontal detachment and steep ramp. Therefore, we suggest that Model II or Model III are probable geometric simplifications of the more complex exhumation of the RMCC.

4. Conclusions

1. The fault geometry and the velocity field have a first-order effect on the temperature distribution during normal faulting. Increasing the rate of extension and faulting dip angles enhances the surface heat flow. However, the peak heat flow is not necessarily centered on the fault tip. Low-angle normal faults with erosion of the footwall show generally higher surface heat flow values in the footwall. If the geometry of normal faulting is similar to the antiformal hinge line migration model, the near-surface heat flow on the footwall side relaxes to lower values during extension resulting in concave-upwards heat flow versus distance to fault tip curves. Therefore, low-angle normal faults with antiformal hinge line migration show generally higher heat flow values in the hanging wall. If the fault slip is large enough (i. e. several tens of kilometers), if the dip of the normal fault exceeds 10° to 15° and if only mid-crustal metamorphic rocks are exposed in the metamorphic core, a ramp-flat geometry of the normal fault has to be considered. A pronounced near-surface heat flow peak that is centered near the fault tip characterizes ramp-flat detachments with kink-band geometry. Again the heat flow in the footwall relaxes to lower values as the material moves away from the fault tip resulting in convex upwards curves in a plot of distance to fault tip versus heat flow. The width of the conductive thermal overprint of the hanging wall is – besides the extension rate – a function of the width of the kink-band and thus of the dip of the ramp. Steep-dipping ramps result in higher peak heat flows but more narrow zones of thermal overprint of the hanging wall. As a rule of thumb, for extension rates on the order of several mm/a, the width of the thermal welt of about 20 mW/m² is equal to the horizontal distance between the antiformal and synformal hinge.

Table 2
Apatite FT results from the surrounding of the Rechnitz Metamorphic Core Complex.

code	locality	petrography	cryst.	spontaneous		induced		dosimeter		$P(\chi^2)$	FT-age	
				ρs	(Ns)	ρi	(Ni)	ρd	(Nd)	[%]	[Ma±1σ]	
GP-19	Zöbern	conglomerate	60	7.9	(2732)	16.3	(5653)	4.66	(9076)	3	42.0±2	**central age**
GP-20	Boden	conglomerate	50	4.8	(1274)	8.7	(2322)	4.56	(4537)	35	46.6±2	**pooled age**
GP-21	Ransdorf	orthogneiss	30	6.6	(953)	9.1	(1283)	4.48	(10915)	59	61±8	**pooled age**

Cryst.: number of dated apatite crystals.
Track densities (ρ) are as measured (x10^5 tr/cm^2); number of tracks counted (N) shown in brackets.
*: Central ages calculated using dosimeter glass: CN 5 with zCN5 = 373 ± 7 with the method of Galbraith and Laslett (1993).
$P(\chi^2)$: probability obtaining Chi-square value for υ degree of freedom (where υ = no. crystals-1).

Although the position of the peak heat flow will be always somewhere near the fault tip, its exact location is again dependent on the geometry of the detachment. Low-angle ramps, which dip with less than around 20°, will have a near-surface peak heat flow on the hanging wall side. About 30°-dipping ramps have a typically centered peak on the fault tip. Steep ramps dipping with more than 40° have a near-surface maximum heat flow located in the footwall. Note, that this is only true for the geometries where the thickness of a given rock layer is conserved (e. g. kink-band geometry, flexural failure model). If the axial planes of the antiformal and synformal hinges are always vertical as in the subvertical simple shear model the near-surface heat flow peak will be always on the hanging wall side near the fault tip.

2. Near-surface heat flow measurements over active detachments can provide important information on the geometry of the normal fault. During rapid tectonic movement of rocks heat advection is the dominant first-order mechanism, which affects the temperature distribution within the crust. After the tectonically active period, numerous processes can influence the lateral distribution of the near-surface heat flow including for example igneous activity, thermal disturbance by moving water or heat production by heterogeneously distributed radioactive elements (LACHENBRUCH et al., 1994; SASS et al., 1994). Therefore, only methods recording the temperature distribution during tectonic activity (e. g. thermochronological and petrological methods) can reveal the thermal overprint of the hanging wall above inactive metamorphic core complexes.
3. Rocks exhuming from below a low-angle normal fault and a ramp-flat detachment reveal totally different cooling history in the footwall. In the low-angle normal fault model a given rock volume from the footwall steadily cools during extension and consequently the time when the rock sample is at its peak temperature is before the onset of extension. Rocks below an active horizontal detachment suffer initially no significant temperature change. When the rock volume approaches the synformal hinge line, the rocks are heated by conduction from beneath the ramp. Below the ramp the rock sample is exhumed and cools steadily. Thus a local temperature maximum or probably the peak temperature is reached during extension.
4. At the margin of the RMCC the heat flow distribution of the steeper ramp geometry (Model III) gives the best fit to the evidence available of the thermal history of the region. Although the window is partly surrounded by deep basins and thus no straight strike profile is available for analyses, scattered borehole and surface samples reveal a thermal overprint only in the close neighborhood of the footwall exposures.

5. Acknowledgment

B. G. developed the used computer software with funding from project P-14129-GEO and P-15668-GEO of the *Austrian Science Fund* (FWF) and the *Hochschuljubiläumsstiftung der Stadt Wien*. The *German Science Foundation* financed the fission track part of this study in the frame of the Collaborative Research Centre 275. Donna WHITNEY, David FOSTER and Annia FAYON are thanked for comments on an earlier version of this manuscript. Thoroughly reviews of an anonymous reviewer, Fritz KOLLER and the editor Volker HÖCK helped to clarify the ideas presented in this work.

References

AXEN, G. J. & BARTLEY, J. M., 1997: Field tests of rolling hinges: Existence, mechanical types, and implications for extensional tectonics. – J. Geophys. Res., **102,** 20515-20537.

BELOCKY, R., SACHSENHOFER, R. F. & POHL, W., 1991: Neue Argumente für eine miozäne epithermale Genese der Antimonerzlagerstätte Schlaining (Burgenland/Österreich): Flüssigkeitseinschlußuntersuchungen und das Inkohlungsbild der benachbarten Tertiärbecken. – Berg- und Hüttenmänn. Mh., **136,** 209-213.

BALOGH, K. & DUNKL, I., submitted: Chronology of Alpine metamorphism and exhumation of the Austroalpine basement in the Sopron Mts. (Eastern Alps, Hungary) – Thermochronology or mineral growth? – Mineral. Petrol.

BUCK, W. R., 1988: Flexural rotation of normal faults. – Tectonics, **7,** 959-973.

BUCK, W. R., MERTINEZ, F., STECKLER, M. S. & COCHRAN, J. R., 1988: Thermal consequences of lithospheric extension: pure and simple. – Tectonics, **7,** 213-234.

CARSLAW, S. & JAEGER, J. C., 1959: Conduction of Heat in Solids. – 510 S., New York (Oxford University Press).

CLIFF, R. A., DROOP, G. T. R. & REX, D. C., 1985: Alpine metamorphism in the south-east Tauern Window, Austria: 2. Rates of heating, cooling and uplift. – J. Metamorph. Geol., **3,** 403-415.

DAVIS, G. H., 1983: Shear zone model for the origin of metamorphic core complexes. – Geology, **11,** 342-347.

DODSON, M. H., 1973: Closure temperature in cooling geochronological and petrological systems. – Contrib. Mineral. Petrol., **40,** 259-274.

DONELICK, R. A., KETCHAM, R. A. & CARLSON, W. D., 1999: Variability of apatite fission track annealing kinetics II: Crystallographic orientation effects. – Am. Mineral., **84,** 1224-1234.

DUNKL, I. & DEMÉNY, A., 1997: Exhumation of the Rechnitz Window at the border of Eastern Alps and Pannonian basin during Neogene extension. – Tectonophysics, **272,** 197-211.

DUNKL, I., GRASEMANN, B. & FRISCH, W., 1998: Thermal effects of exhumation of a metamorphic core complex on hanging wall syn-rift sediments – an example from the Rechnitz Window, Eastern Alps. – Tectonophysics, **297,** 35-50.

EBNER, F. & SACHSENHOFER, R. F., 1991: Paleogeography, subsidence and thermal history of the Neogene Syrian basin (Pannonian basin system, Austria). – Tectonophysics, **242,** 133-150.

FITZGERALD P. G. & GLEADOW A. J. W., 1988: Fission track geochronology, tectonics and structure of the Transantarctic Mountains in Northern Victoria Land, Antarctica. – Chem. Geol., **73,** 169-198.

FLÜGEL, H. W. & NEUBAUER, F., 1984: Geologische Karte der Steiermark 1:200.000. – Mitt. Abt. Geol. und Paläont. Landesmuseum Joanneum, 45 S.

GALBRAITH, R. F. & LASLETT, G. M., 1993: Statistical models for mixed fission track ages. – Nucl. Tracks Radiat. Meas., **21,** 459-470.

GIBBS, A. D., 1984: Structural evolution of extensional basin margins. – J. Geol. Soc. London, **141,** 609-620.

GLEADOW, A. J. W., DUDDY, I. R. & LOVERING, J. F., 1983: Fission track analysis: a new tool for the evaluation of thermal histories and hydrocarbon potential. – Australian Petrol. Explor. Assoc. J., 23, 93-102.

GRASEMANN, B. & MANCKTELOW, N., 1993: Two-dimensional thermal modeling of normal faulting: the Simplon Fault Zone, Central Alps, Switzerland. – Tectonophysics, **255,** 155-165.

HARRISON, T. M., ARMSTRONG, R. L., NAESER, C. W. & HARAKAL, J. E., 1979: Geochronology and thermal history of the Coast Plutonic Complex, near Prince Rupert, British Columbia. – Can. J. Earth Sci., **16,** 400-410.

HERRMANN, P. & PAHR, A., 1988: Gelogische Karte der Republik Österreich, 1:50000, Erläuterungen zu Blatt 138 Rechnitz. – Geol. B.-A., Wien, 40 S.

HOISCH, T. D., Wells, M. L. & Wolff, E. D., 1997: Two-dimensional thermal models of detachment faulting with application to the Raft River detachment in northwest Utah. – GSA Abstracts with Programs. **29,** A-381.

HORVÁTH, F., 1993: Towards a mechanical model for the formation of the Pannonian basin. – Tectonophysics, **226,** 333-357.

HURFORD, A. J., 1986, Cooling and uplift patterns in the Lepontine Alps South Central Switzerland and an age of vertical movement on the Insubric fault line. – Contrib. Mineral. Petrol., **93,** 413-427.

KETCHAM, R. A., 1996: Thermal models of core-complex evolution in Arizona and New Guinea: Implications for ancient cooling paths and present-day flow. – Tectonics, **15,** 933-951.

KETCHAM, R. A., DONELICK, R. A. & DONELICK, M. B., 2000: AFTSOLVE: A program for multi-kinetic modeling of apatite fission-track data. – Geological Materials Research. Geolog. Mat. Res., **2,** 1-32.

KING, G. & ELLIS, M., 1990: The origin of large local uplift in extensional regions. – Nature, **348,** 689-693.

KOLLER, F., 1985: Petrologie und Geochemie der Ophiolite des Penninikums am Alpenostrand. – Jb. Geol. B.-A., **128,** 83-150.

LACHENBRUCH, A. H., Sass, J. H. & Morgan, P., 1994: Thermal regime of the southern Basin and Range Province; 2, Implications of heat flow for regional extension and metamorphic core complexes. – J. Geophys. Res., **99,** 22121-22133.

LISTER, G. S. & DAVIS, G. A., 1989: The origin of metamorphic core complexes and detachment faults formed during Teriary continental extension in the northern Colorado River region, U.S.A.. – Jour. Struct. Geol., **11,** 65-94.

MANCKTELOW, N. & GRASEMANN, B., 1997: Time-dependent effects of heat advection and topography on cooling histories during erosion. – Tectonophysics, **270,** 167-195.

MÜLLER, W., DALLMEYER, R. D., NEUBAUER, F. & THÖNI, M., 1992: Chronology of Variscan metamorphic events and low grade Alpine overprint in the eastern Lower Austroalpine Units: Rb/Sr and 40Ar/39Ar age data (Wechsel and Raabalpen unit, Eastern Alps). – Terra Abstract, **4,** 46.

NEUBAUER, F. & FRISCH, W., 1993: The Austroalpine metamorphic basement east of the Tauern window. – In: J. F. VON RAUMER & F. NEUBAUER (eds): Pre-Mesozoic geology of the Alps. 515-536, Heidelberg (Springer Verlag).

NEUBAUER, F., DALLMEYER, R. D., DUNKL, I. & SCHIRNIK, D., 1995: Late Cretaceous exhumation of the metamorphic Gleinalm Dome, Eastern Alps: kinematics, cooling history, and sedimentary response in a sinistral wrench corridor. – Tectonophysics, **242,** 79-98.

OZISIK, M. N., 1985: Heat Transfer. – 576 S., New York (McGaw-Hill).

PAHR, A., 1980: Die Fenster von Rechnitz, Berstein und Moltern. – In: Oberhauser, R. (ed.): Der Geologische Aufbau Österreichs, 77-91, Vienna (Springer).

PAHR, A., 1984: Gelogische Karte der Republik Österreich, 1:50000, Erläuterungen zu Blatt 137 Oberwart. – Geol. B.-A., Wien, 47 S.

PEACEMAN, D. W. & RACHFORD, H. H., 1955: The numerical solution of parabolic and elliptic differential equations. – Jour. Ind. Math. Soc., **3,** 28-41.

PRAUS, O., PEČOVA, J. P. V., BABUŠKA, V. & PLOMEROVÁ, J., 1990: Magnetotelluric and seismological determination of lithosphere-asthenosphere transition in Central Europe. – Phys. Earth Planet. Inter., **60,** 212-228.

PURDY, J. W. & JÄGER, E., 1976: K-Ar ages on rock-forming minerals from the Central Alps. – University of Padova, Mem. Ist. Geol. Mineral., **30,** 32 p.

RAMSAY, J. G. & HUBER, I. M., 1987: The Techniques of Modern Structural Geology. Volume 2: Folds and Fractures. – 381 S., London (Academic Press Inc. Ltd).

RATSCHBACHER, L., BEHRMANN, J. H. & PAHR, A., 1990: Penninic windows at the eastern end of the Alps and their relation to the intra-Carpathian basins. – Tectonophysics, **172,** 91-105.

RATSCHBACHER, L., FRISCH, W. & LINZER, H.-G., 1991: Lateral extrusion in the Eastern Alps, Part 2: structural analysis. – Tectonics, **10,** 257-271.

RUPPEL, C., ROYDEN, L. & HODGES, K.V., 1988: Thermal modeling of extensional tectonics: application to pressure-temperature-time histories of metamorphic rocks. – Tectonics, **7,** 947-957.

SACHSENHOFER, R. F., 1991: Maturität im Steirischen Tertiärbecken. – Erdöl Erdgas Kohle, **107,** 12-17.

SACHSENHOFER, R. F., 2001: Syn- and post-collisional heat flow in the Cenozoic Eastern Alps. – Int. Journ. Earth Sciences, **90,** 579-592.

SASS, J. H., LACHENBRUCH, A. H., GALANIS JR., S. P., MORGAN, P., PRIEST, S. S., MOSES JR., T. H. & MUNROE, R. J., 1994: Thermal regime of the southern Basin and Range Province: 1 Heat flow data from Arizona and the Mojave Desert of California and Nevada. – J. Geophys. Res., **99,** 22093-22119.

SCHÖNLAUB, H. P., 2000: Burgenland – Erläuterungen zur Geologischen Karte des Burgenlandes 1:200000. – Geol. B.-A., 130 S.

SELVERSTONE, J., 1985: Petrologic constraints on imbrication, metamorphism and uplift in the SW Tauern Window, Eastern Alps. – Tectonics, **4,** 687-704.

SELVERSTONE, J., AXEN, G. J. & BARTLEY, J. M., 1995: Fluid inclusion constraints on the kinematics of footwall uplift beneath the Brenner Line normal fault, eastern Alps. – Tectonics, **14,** 264-278.

SPENCER, J. E., 1984: Role of tectonic denudation in warping and uplift of low-angle normal faults. – Geology, **12,** 95-98.

STÜWE, K. & SANDIFORD, M., 1995: Mantle-lithospheric deformation and crustal metamorphism with some speculations on the thermal and mechanical significance of the Tauern Event, Eastern Alps. – Tectonophysics, **242,** 115-132.

TARI, G., 1994: Alpine tectonics of the Pannonian basin. – [Ph.D. thesis]: 501 S. Houston (Rice University).

TARI, G. & HORVÁTH, F., 1995: Middle Miocene extensional collapse in the Alpine-Pannonian transition zone. – In: HORVÁTH, F., TARI, G. & BOKOR, Cs. (eds), Extensional collapse of the Alpine Orogene and hydrocarbon prospects in the basement and basin fill of the western Pannonian basin. 75-105, Nice (AAPG International Conf., Guidebook to fieldtrip No. 6).

TER VOORDE, M. & BERTOTTI, G., 1994: Thermal effects of normal faulting during rifted basin formation, 1. A finite difference model. – Tectonophysics, **240,** 133-144.

TURCOTTE, D. L. & SCHUBERT, G. 1982. Geodynamics – Applications of continuum physics to geological problems. – 450 S., New York (John Wiley & Sons).

TWISS, R. J. & MOORES, E. M., 1992: Structural Geology. – 532 S., New York (W. H. Freeman and Company).

VAN WEES, J. D., DE JONG, K. & CLOETHING, S., 1992: Two-dimensional P-T-t modelling and the dynamics of extension and inversion in the Betic Zone (SE Spain). – Tectonophysics, **203,** 305-324

VON BLANKENBURG, F., VILLA, I. M., BAUR, H., MORTEANI, G. & STEIGER, R. R., 1989: Time calibration of a PT-path from the Western Tauern Window, Eastern Alps: The problem of closure temperatures. – Contrib. Mineral. Petrol., **101,** 1-11.

WAGNER, G. A., REIMER, G. M. & JÄGER, E., 1977: Cooling ages derived by apatite fission-track, mica Rb-Sr and K-Ar dating: the uplift and cooling history of Central Alps. – University of Padova, Mem. Ist. Geol. Mineral., **30,** 1-27.

WERNICKE, B. & AXEN, G. J., 1988: On the role of isostasy in the evolution of normal fault system. – Geology, **16,** 848-851.

Appendix

The time-dependent heat transfer equation in two-dimensions including heat conduction, advection and production but for incompressible conditions is:

$$\frac{\partial T}{\partial t} = \kappa\left(\frac{\partial^2 T}{\partial x^2} + \frac{\partial^2 T}{\partial z^2}\right) + \left(v_x \frac{\partial T}{\partial x} + v_z \frac{\partial T}{\partial z}\right) + \frac{A_{(z,t)}}{\rho C} \qquad (A1)$$

where T = temperature [°C]
t = time [s]
k = thermal diffusivity [m²/s]
x, z = horizontal and vertical (i.e. depth) direction [m]
vx, vz = velocities in x and z direction [m/s]
$A_{(z,t)}$ = volumetric heat production [W/m³]
C = specific heat [J/kgK]
ρ = density [kg/m³]

In the presented model the volumetric heat production is not a constant value but an exponential function where the heat generation decays with depth:

$$A_{(z,t)} = A_0 \exp\left(\frac{-z}{l_{(t)}}\right) \qquad (A2)$$

where A_0 is the heat generation in the surface layer, $l_{(t)}$ is the variable depth at which the heat production drops to 1/e of this surface value.

This system is solved numerically in two dimensions using an ADI (alternating-direction-implicit) method with a two-step scheme (PEACEMAN & RACHFORD, 1955). The advective term has to be discretize separately using an upwind differencing scheme, which applies backward or forward differencing depending on the sign of the velocity vector (OZISIK 1985). This procedure is only stable as long as:

$$\Delta t \le \left\{\frac{|v_x|}{\Delta x} + \frac{|v_z|}{\Delta z} + \frac{2\kappa}{(\Delta z)^2}\right\}^{-1} \qquad (A3)$$

The other boundary conditions are:

$$T = T_s = 0 \qquad (A4)$$

at the upper boundary where T_s is the constant surface temperature,

$$\frac{dT}{dx} = 0 \qquad (A5)$$

at the left and right side. The lower boundary condition is a time-dependent function where the temperature at the base of the crust at a given time is calculated using an analytical solution (MANCKTELOW & GRASEMANN, 1997):

$$T(z,t) = \zeta(z,t)\exp\left(-\frac{v_z}{2\kappa}z - \frac{v_z^2}{4\kappa}t\right) + T(z) \qquad (A6)$$

where $T(z)$ is the steady state solution:

$$T(z) = \beta\left[1 - \exp\left(-\frac{z}{l}\right)\right] + \gamma\left[1 - \exp\left(-\frac{v_z}{\kappa}z\right)\right] \qquad (A7)$$

where:

$$\beta = \frac{A\,l^2}{\rho\,C(\kappa - v_z\,l)} \qquad \gamma = \frac{T_l - \beta\left[1 - \exp\left(-\frac{L}{l}\right)\right]}{1 - \exp\left(-\frac{v_z}{\kappa}L\right)}$$

A solution for the time and position dependent is given by CARSLAW & JAEGER (1959):

$$\zeta(z,t) = \frac{2}{L}\sum_{n=1}^{\infty}\exp\left(-\kappa\,\omega_n{}^2 t\right)\sin\omega_n z \int_0^L \zeta(z', t=0)\sin\omega_n z'\,dz' \qquad (A8)$$

where: $\omega_n = \frac{n\pi}{L}$

Finite difference solutions for zero horizontal velocities and for vertical exhumation of the whole crust (hanging wall and footwall) in the z direction where compared with the analytical solutions in order to check the validity and accuracy of the numerical approximation.

Manuscript received: 17. 09. 2001 ●
Revised version received: 13. 03. 2003 ●
Manuscript accepted: 25. 03. 2003 ●